Cytometry Part B (Clinical Cytometry) 72B:63–76 (2007)

"Virtual Flow Cytometry" of Immunostained Lymphocytes on Microscopic Tissue Slides: *i*HCFlow™ Tissue Cytometry

Hernani D. Cualing,[1,2]* Eric Zhong,[2] and Lynn Moscinski[1]

[1]H. Lee Moffitt Cancer Center and Research Institute, University of South Florida, Tampa, Florida

[2]IHCFLOW-GreenGreat, New Jersey

Background: A method and approach is developed for fully automated measurements of immunostained lymphocytes in tissue sections by means of digital color microscopy and patent pending advanced cell analysis. The validation data for population statistic measurements of immunostained lymphocytes in tissue sections using tissue cytometry (TC) is presented. The report is the first to describe the conversion of immunohistochemistry (IHC) data to a flow cytometry-like two parameter dot-plot display, hence the technique is also a virtual flow cytometry. We believe this approach is a paradigm shift, as well as novel, and called the system *i*HCFlow™ TC. Seven issues related to technical obstacles to virtual flow cytometry (FC) are identified.

Design: Segmentation of a 512 × 474 RGB image and tabular display of statistical results table took 12–15 s using proprietary developed algorithms. We used a panel of seven antibodies for validation on 14 cases of mantle cell lymphoma giving percentage positive, total lymphocytes, and staining density. A total of 2,027 image frames with 810,800 cell objects (COBs) were evaluated. Antibodies to CD3, CD4, CD8, Bcl-1, Ki-67, CD20, CD5 were subjected to virtual FC on tissue. The results of TC were compared with manual counts of expert observers and with the results of flow cytometric immunophenotyping of the same specimen.

Results: The correlation coefficient and 95% confidence interval by linear regression analysis yielded a high concordance between manual human results (M), FC results, and TC results per antibody, (r = 0.9365 M vs. TC, r = 0.9537 FC vs. TC). The technical issues were resolved and the solutions and results were evaluated and presented.

Conclusion: These results suggest the new technology of TC by *i*HCFlow™ could be a clinically valid surrogate for both M and FC analysis when only tissue IHC is available for diagnosis and prognosis. The application for cancer diagnosis, monitoring, and prognosis is for objective, rapid, automated counting of immunostained cells in tissues with percentage results. We report a new paradigm in TC that converts IHC staining of lymphocytes to automated results and a flow cytometry-like report. The dot plot histogram display is familiar, intuitive, informative, and provides the pathologists with an automated tool to rapidly characterize the staining and size distribution of the immunoreactive as well as the negative cell population in the tissue. This systems tool is a major improvement over existing ones and satisfy fully the criteria to perform Cytomics (Ecker and Tarnok, Cytometry A 2005;65:1; Ecker and Steiner, Cytometry A 2004;59:182–190; Ecker et al., Cytometry A 2004;59:172–181). © 2006 Clinical Cytometry Society

Key terms: tissue cytometry; cytomics; virtual flow cytometry; immunohistochemistry; image understanding; image analysis; high throughput analysis

We developed a method and apparatus that perform image analysis of immunohistochemically stained tissue using the *i*HCFlow™ system approach. The objective was to recreate the functionality of a flow cytometer, but instead of using the requisite cell suspension specimen, we have developed an approach to be applied directly to stained microscopic slides with tissue sections. We have identified and offered solutions to seven critical problems in performing virtual flow cytometry (FC) on immuno-

*Correspondence to: Hernani Cualing, H. Lee Moffitt Cancer Center and Research Institute, University of South Florida, Tampa, FL, USA.

E-mail: cualinhd@moffitt.usf.edu

Received 21 February 2006; Revision 8 August 2006; Accepted 22 August 2006

Published online 28 November 2006 in Wiley InterScience (www.interscience.wiley.com).

DOI: 10.1002/cyto.b.20148

stained slides. These include: (1) thick tissue sections with overlapping of cells, (2) variability and lack of standardization of immunostaining of tissues, (3) optimal sampling resolution for obtaining size and staining data per cell object, (4) lack of a simple preprocessing technique utilizing optical output properties of image acquisition hardware, (5) underdeveloped cell-based algorithms able to detect dual populations (positive immunostained cells and nonimmunostained relevant cells of the same class) and, (6) lack of knowledge on standardizing threshold cut off to compensate for variability of staining and, (7) lack of a cell-based approach that automatically identifies the image specific parameter that optimizes detection of percentage positive cells. We present solutions to the above issues.

The hematopathologist's standard of clinical practice in most patient's reports is to estimate the percentage of immunohistochemically stained cells and report the visual or manual estimate. This practice is subjective and often gives a wide range of results that depends on the level of the microscopists' skill. This is due to the difficulty in counting positive cell objects (COBs) accurately because of overlapped stained nuclei, variability of immunostaining, and the limitation of our visual system. Given the top administrative priority of minimizing medical errors in medicine in general, developing a tool in diagnostic pathology that promises similar objectivity as flow cytometry, will only decrease the incidence of errors in diagnosis.

We applied a novel, useful, and accurate algorithm that was made feasible after resolving the issues of performing a population or cell-based analysis and contributed to advances in cytomics (1–5). Using tissue immunohistochemistry (IHC) and *i*HCFlow™ approach, we produced results similar to FC dot-plot histograms. These results, along with a table, are familiar and provide an objective percent positive and negative count of tissue IHC to the diagnostic pathologists and hematologist-oncologists. This tool promises to enhance accuracy of diagnosis, disease monitoring, and prognostication, as well as research reporting in lymphoid histology and pathologic disorders.

DESIGN

Materials

Formalin-fixed paraffin embedded blocks of tissue were used for this study. We used seven monoclonal antibodies for validation on each of 14 cases of excised lymph nodes obtained for the diagnosis of lymphoma. A total of 2,027 image frames with 810,800 COBs were evaluated. Membrane reactive antibodies to T cell associated markers CD3, CD4, CD5, and CD8 were analyzed. For B cells, a reactive monoclonal antibody, CD20 (L26, mature B cells), was used. These corresponding antibodies were run in parallel in FC and results correlated with tissue immunoreactivity obtained using *i*HCFlow™ tissue cytometry (TC). Nuclear reactive antibodies to Bcl-1(cyclin D1, mantle cell lymphoma and others) and Ki-67 (Mib-1, proliferative marker) were analyzed by TC only. All paraffin-embedded tissue sections were fixed in neutral buffered formalin, processed in a VIP tissue processor, and microtome sectioned at 2 μm thickness to minimize overlapping nuclei, and oven-dried on + charged slides. IHC was performed using a Benchmark automated IHC system (Ventana Medical Systems, Tuczon, AZ) with the following conditions: Bcl-1 (clone p2d11f11, predilute Ventana with protease and CC1 heat-induced epitope retrieval HIER), CD3 (PS1 predilute Ventana Trilogy HIER), CD4 (1F6, 1:10 CC1 amplification, Zymed), CD5 (4c7, 1:25, Novocastra, Trilogy HIER), CD8 (1a5, 1:25 CC1 HIER, Zymed), CD20 (L26, predilute CC1 HIER), Ki67 (MM1, predilute CC1 HIER). Mayer Hematoxylin was applied using the autostainer for 10 min extended time as a blue nuclear counterstain.

Methods

Microscopy and image frame information. The slides were examined using a Leica brightfield microscope with a 20× objective, and images captured with an Insight color CCD (Diagnostic Instruments, Westlar, Germany), running Spot software version 3.4 for Windows NT 2000. The camera CCD photoreceptive field (1,060 × 1,020 pixels) was by software-mode trimmed to 512 × 474 pixels for dimensionality reduction, optimal object size, and for computational efficiency. The images were stored as either a JPEG or PICS file and analyzed using a previously developed advanced cell imaging software. No interactive labeling or manual shading or color correction was performed on images. The light intensity rheostat was set to 7.0 of 12.0. The light source was 30 W 12 V incandescent bulb with a blue filter (80a Tiffen), collimated through a condenser aperture set at 0.5 ph, under Kohler illumination, and using a 20× nplan 0.4 *na* objective without magnification in the trinocular adapter. The camera has a single CCD with interpolated red, green, blue filters overlying each pixel. The pixel size was1.5 pixels per micron for the 512 × 474 pixels image frame. Image acquisition was manual and on selected lymphoid rich areas. In these areas, 3-dimensional nuclei were tangentially cut in thin histologic sectional planes resulting in random nuclear tangents of varying diameter (6). The images were manually focused, captured, and saved. Result for the 15 image frames was recorded per antibody with an average 7,500 total cell analyzed. Each image file was 711 kb in PICS format. Each image frame took 12–15 s from start of analysis to generation of the statistical table and correlated dot plot histogram display. A new and enhanced rapid version takes a JPEG formatted image and took 2–3 s from start to display of results.

Virtual FC algorithm. The algorithm is outlined in Table 1. The software used to analyze the images was prototyped and developed by IHCFLOW-GreenGreat.

For the image frame using the above 20× set up, the pixel size converts to 2/3 μm/pixel. The formula below was used to convert pixel area to cell diameter in microns (*Y* data):

$$\begin{aligned}\text{Cell diameter} &= 2 \times (\text{sqrt of } (\text{area in pixels}/\pi))/1.5 \\ &= \text{sqrt of } (\text{area in pixels} \times P) \quad (1)\end{aligned}$$

The intensity component of the colored blue and brown objects were summed up per cell object, averaged, and stored, and converted as average stain density (*X* data).

Table I
Summary of the Software Algorithm for i*HCFlow*^{TM} *Tissue Cytometry*

Given *x, y* as the pixel spatial coordinate in the image frame of an arbitrary image *A* with RGB information representing the original color image.
This image is subjected to contrast intensity enhancement using red and blue CCD channels.
The Red channel is used to enhance blue nuclei and Blue channel is used to enhance brown stained cell objects.
Objects masks of same class of cells selected using automated thresholding by isodata.
Calculation of the parameter χ for entropy mode thresholding.
Secondary extraction of dominant hue and dominant intensity from above masks using combined percentile, isodata, and entropy thresholding.
The masks are refined by thresholding only in hue and intensity using entropy χ mode with prior removal of pixel singularities.
More refinement of the masks using linking and filling voids.
Dynamic thresholding using size information to select single cells of same class.
Cellular logic used to refine objects and discard non objects further.
Declumping subroutine combined with spatial criteria.
Size information and cell object densities are stored per cell.
Counting cell objects with corresponding size and object densities per cell.
Statistical cytometry results on a table or plot the density versus cell size.

The *X* data were obtained as follows. Each nuclei object was labeled and counted as an event for the virtual flow cytometry. The RGB COBs were converted to Hue, Saturation, Intensity image planes. The transmitted light decreased in proportion to the amount of stain pigments as they passed through the optics and through the stained cells imparting a numerical representation of light intensity per pixel of the cell objects. The intensity component of all pixels, objects and nonobjects, from here on, was converted to density. The optical density data per cell object was given by the sum of optical density of the pixels comprising the previously labeled COBs. Each cell object was then labeled and contained size and density numbers which were used for the dot plot display COB. The final resulting data then consisted of an array of labeled objects with size and corresponding stain density. These two parameters defined the frequency distribution of the COBs in the two dimensional dot plot.

For terminology, we designated cells or nuclei as representing histologically stained cells and COBs as the digital representation of those cells. COBs was the term applied to digitized pixels of nuclear objects and also excluded the background nonobject pixels. The nonobject pixels were not used in the calculations.

Flow cytometry. The tissues for FC were prepared using a Becton Dickinson Medimachine System which is a safe, standardized sample preparation system for the automated and mechanical disaggregation of solid tissues for flow cytometric analysis. The suspension was needled using a 23 × 1½ needle to eliminate sample clumping and aggregation. The cell suspension was then filtered through a Filcon with the appropriate pore size (50-mm Filcons are suitable for most tissues, e.g. lymph nodes, tumors, and skin). Cell count and viability using Trypan Blue were performed for assessment of the sample. The cell concentration was adjusted to 5×10^5 or 1×10^6 cells/ml. Staining of the cells by a direct method was used to detect cells bearing specific membrane antigens. This was done by treating a patient's cell population with monoclonal antibodies conjugated to a variety of different fluorescent tags. The antibodies were added directly to the tubes containing the appropriate cell concentration and incubated at room temperature in the dark for 20 min. The tubes were then washed with 2 ml of 1% PBS for 5 min at 1,500 rpm. The supernatant was decanted and the pellet was resuspended by adding 0.5 ml of 1% paraformaldehyde. The tubes were gently vortexed and placed at 2°–8° until ready to be run on the Flow Cytometer. Analysis was done using logical gating on lymphocyte gate counting 5,000 events. A Becton Dickinson FacsCalibur with CellQuest software version 3.2.1 was used for four color acquisition and analysis. Membrane reactive antibodies to T-cell associated markers/clone names with fluorophores [CD3 PerCP-Cy5.5 (SK7), CD4 FITC (SK3), CD5 APC (L17F12), and CD8 APC (SK1)] were used. CD20 APC (L27, mature B cells) was also used.

Manual quantitation. The identical sections used for TC were manually evaluated by microscopy. Five-hundred cells were quantitated as positive or negative cells for each antibody and tabulated. All results were averaged by a single expert hematopathologist.

Statistical analysis. Linear regression analysis and 95% confidence interval were employed to correlate manual quantitation, flow cytometry, and TC results (GraphPad, Instat3 v 3.06 32 bit). Since the result of FC was known for most antibody per case, linear regression analysis was performed to correlate with TC and manual counting.

The coefficient of variation was calculated using the formula below and numbers of positive cells were used for x obtained over a range of 10–24 image frames with an average of 15 frames per slide:

$$\text{C.V.} = \frac{\text{standard deviation}}{\text{Mean}}, \text{ where the SD} = \text{sqrt}(\Sigma(x - X)^2/n) \quad (2)$$

Image processing. Three segmentation modes were used to obtain robust, accurate, interactive cell-based segmentation using multiple layers of auto-thresholding to identify single cells belonging to one class: one stained, the other unstained. The first mode maximized the differential contrast between the positive brown COBs and the negative blue COBs, and resulted in a preliminary region of interest. The second mode performed color and density equalization or normalization in global and region of interest images, by percentile thresholding the preliminary region passed from the first mode to get a combined region of blue and brown stained COBs. The third mode

automatically adjusted the sensitivity "gate" for positive COBs by a combination of isodata thresholding, automated image-based and parameterized entropy thresholding, and recursive region of interest cellular logic thresholding. As an output of the third mode we obtained a non-blue mask, and by applying the mask to the intermediate result of the second mode, we finally segmented separate groups of blue and brown COBS. The image processing algorithm uses auto-thresholding on red and blue channels in RGB to get the raw working image of all cells, and then refines the working image with thresholding on hue and intensity channels in HS I, and further separates different classes of cells by auto-thresholding within the working image region.

First segmentation mode: Density contrast. The first mode was based on RGB channel enhanced contrast using the output of the complementary color channel. This preprocessing step was termed "RGB channel enhancement." The channel separation was performed automatically by hardware via the CCD camera three channel output. Contrast refers to the range of brightness of the image, i.e. the difference between the brightest part and the darkest part. However, contrast also occurs at the boundaries between blocks of color, usually the edges of objects. This boundary definition allows selection of objects. Objects selection was automated by utilizing the RGB channel from the camera CCD that was complementary to the color of the chromogen positive cell object that we were segmenting from other COBs and from the background. Our objective was to segment both the brown and the blue stained COBs (negative nuclei) and separate them both from the background. For example, the complementary color channel nearest to the brown stained cells was the blue channel. Similarly, for the blue stained nuclei, the complementary color was the red channel. As shown empirically and by measurements below, the blue channel provided the maximum contrasts to distinguish the brown COBs from the blue COBs. The red channel likewise provided the maximum contrasts that distinguished both the brown and the blue COBs from the background.

The contrast analysis procedure is as follows. The density distribution of pixels of COBs was obtained using the plot menu histogram profile function of NIH Image J (NIH W Rasband, v1.34m). A line drawn across a cell object produced a frequency histogram of pixel density along the drawn line. For this procedure, a monochromatic channel image was displayed on the screen. Then the histogram profile function was activated followed by selection of a line tool. A finite line was drawn from at least two COBs: one corresponding to the brown stained cell and the other to the unstained nuclei. The density distribution was displayed on a plot. The minimum value along the section of the brown cell object and the maximum value from the blue cell object were used for the calculation of the difference in contrasts representing the I_{minbrown} and I_{maxblue}, respectively [see Eq. (5) below]. We chose these values to get the conservative number among a set comprising the difference between brown and blue cell objects. The larger this contrast value, the higher the difference between the optical densities of that blue and brown COBs.

The general equation for contrasts was given by:

$$\text{Percent contrast } (C\%) = \frac{(I_{\max} - I_{\min}) \times 100}{I_{\max} + I_{\min}} \quad (3)$$

To include the background in contrast calculation, we used a modified formula (7,8),

$$c\% = \frac{(I_{\max} - I_{\min}) \times 100}{(I_{\max} + I_{\min} + 2v)} \quad (4)$$

where V is the pixel density of background.

We applied the above equation on the actual image, the contrast of Brown and Blue objects in R, G, B channels where $I_{\max}$ and $I_{\min}$ of brown and blue were low maximum of brown and high minimum of blue pixel density number of brown and blue cell objects, respectively.

$$\text{Percent contrasts } (C\%) = \frac{(I_{max\ brown} - I_{min\ blue}) \times 100}{(I_{max\ brown} + I_{min\ blue}) + 2v} \quad (5)$$

Second segmentation mode. The second mode addressed the issue of hue singularity, modulus hue property, and the issue of detecting "pale blue" nuclei by simple thresholding. Hue singularity is a point where hue is undefined at the brightest and darkest range. For example, a brown or blue pixel is not visible in the darkest or brightest display because it cannot be distinguished as a true brown or blue color. This mode was performed using the percentile thresholding function. Setting the percentile cut-offs empirically for the brightest and darkest hue, saturation, and intensity pixels in the image frame normalizes the color and grey scale distribution of image frames captured from different areas and different runs of immunostained slides. The percentile function was set to 95% clipped off 5% pixels in the hue and intensity planes. Thresholding was then performed on the remaining 95% pixels.

The hue and intensity conversion and subsequent percentile thresholding also resulted in enhancing contrast of the "paler" blue nuclei against the background. These blue nuclei objects were saved as intermediate bitplane images along with the saved intermediate bitplane images of the brown cell objects. These intermediate images became the region of interest objects in the subsequent third segmentation mode.

Third segmentation mode. The third mode addressed the issue of determining the inclusion criteria for the positive cells. IHC of tissue often showed discrete brown staining identifying the positive cells clearly from the negative nonimmunoreactive cells. Occasionally, the neoplastic associated changes or for technical reason, lymphocytes may have a range of weak to strong immunostaining. The third mode served to adjust the sensitivity "gate" for positive COBs by using operator determined parameterized entropy thresholding. This parameter labeled as entropy χ could be assigned a value that ranges from 0.01 to close to 0.5. The lower χ value picked up a lower number of brown COBs that were highly "dark brown" in appearance and

excluded the other pale "light brown" staining COBs. The higher χ value lowered the selection criteria to include those pale light brown COBs. The function was automated using the linear relationship between the ratio of the positive staining fraction in the blue channel (using the lowest entropy parameter χ) divided by the total COBs segmented via the red intensity channel, and the result multiplied by 0.49 (the near maximal fraction approaching 0.5).

The equation for χ is given as follows:

$$\chi = \left(\frac{\Sigma N_{1\to n}}{\Sigma D_{1\to n}}\right)(0.49) \qquad (6)$$

where N is the sum of the area of all positive COBs resulting from the blue channel thresholding operation using entropy minimum of 0.01, D is the sum of the area of all positive and nonstained COBs resulting from the red channel and the ratio is normalized to values between 0 and 0.5, both values are binary masks, and n is total pixels in the image frame beginning at 1 to total n.

This ratio served as an automated sensitivity "gate" and in manual mode was similar to the FC technique of manual adjustment of the photomultiplier gain. Manual adjustment is also provided by interactively changing the χ parameter.

The entropy mode is as follows. Gray-value morphologic processing using the entropy thresholding technique was adapted from Johannsen and Bille (9). The method divides the histogram into two parts, minimizing the interdependence between two parts, measured in terms of entropy. The grey level that performs this division will be the threshold value. As a condition, the user may specify the fraction χ of the image that minimally should be assigned to be a foreground object. The algorithm then searches for the minimal entropy within this constraint.

The entropy mode uses a dynamic parameter χ to allow for only a fraction of the hue and intensity detected objects to be segmented as objects and this parameter also relies on the frequency distribution of hue and intensity. This mode is adaptable and varies dynamically adjusting cell staining variation because of biologic or technical differences. This mode uses image to image math. The result of above calculation of two image frames using first the bitplane mask from blue channel divided by the total mask from both the blue and the red channel combined using binary OR. This number is a fraction that is proportional to the entropy mode fractional parameter. The image math result of above is delimited by multiplying with 0.49 and the resulting product is equal to the χ. We have observed a unique property of this fraction which serve to encapsulate the proportional staining of the dark brown objects over the blue objects.

Each of the result of the thresholding operations is stored in a bitplane image used in bitplane sculpting operations and the binary image is also stored and accessible. The sculpting operations are binary mathematical morphology like erosion and dilation. These operations are empirically predetermined, combined sequentially in a new way allowing for dual thresholding of two types of objects as well as the removal of background nonobjects by morphologic operations, and using a "watershed" (10) procedure to separate clumped, aggregated, and overlapping nuclei that remained after the morphologic operations.

To summarize, we use the preprocessing step of RGB channel enhancement to obtain and pass the blue and red channel thresholding result χ to automated thresholding by entropy in the hue and intensity planes of the working images, and further refine the images by bitplane sculpting guided by size and other morphometric criteria to arrive at single cells results, one stained, the rest unstained but more importantly, belonging to the same class of cells. This class is the lymphocyte; an arbitrary class preselected by this algorithm.

Correlation procedure. The manual estimates of immunoreactivity were compared with the results of cell suspension FC and with the results of virtual FC on each of the antibodies and specimen. The comparisons were made to determine if TC could be used as a surrogate technique for manual counts as well as for results of flow cytometry. Manual counting of 500 cells per antibody was used instead of a quick visual estimate of percentage positive cells.

Data table and dot plot histogram generation. Both the positively stained COBs and the unstained nuclei of the same class COBs were sequentially extracted to yield a numerator and denominator to calculate percent positive and total COBs. Stain density was also obtained per COBs and correlated with size. The nuclei diameters ranged from 5 to 35 μm with a 12–15 modal average. The pixel size was converted to microns and the density spread from 0 to 255 where negative COBs events were plotted blue and positive COBs events plotted red. Positivity criteria was determined by a novel automated thresholding as described above.

RESULTS

Single Cell "Events" High Throughput Result

Figure 1 shows the color image frame of tumor infiltrating cell response to mantle cell lymphoma and the image is shown as an example of the type of image used by the algorithm. The brown stained COBs are the reactive cells stained by CD8 antibody and the majority of nonstained blue nuclei were mantle cell lymphoma COBs. Note the tangential random cut sections of the nuclei illustrating the wide range of maximal nuclear size exposed to the stains. These variable sized nuclei serve as "events" representing COBs similar to the FC event driven analysis. Note that the background between the blue and brown cells shows a very faint brownish tint. These intervening pixel areas for the nonnuclear pixels were excluded and not used in the calculation of population statistic. Each image frame contained predominantly lymphocyte COBs and nuclei average 500 cells. Stroma cell nuclei were rare (less than 6%) compared with the number of lymphocyte nuclei, hence, shape parameters were not used to exclude stroma. The COBs were labeled sequentially to identify each object as an event for cell population analysis and display. The size per COBs were obtained using each of the

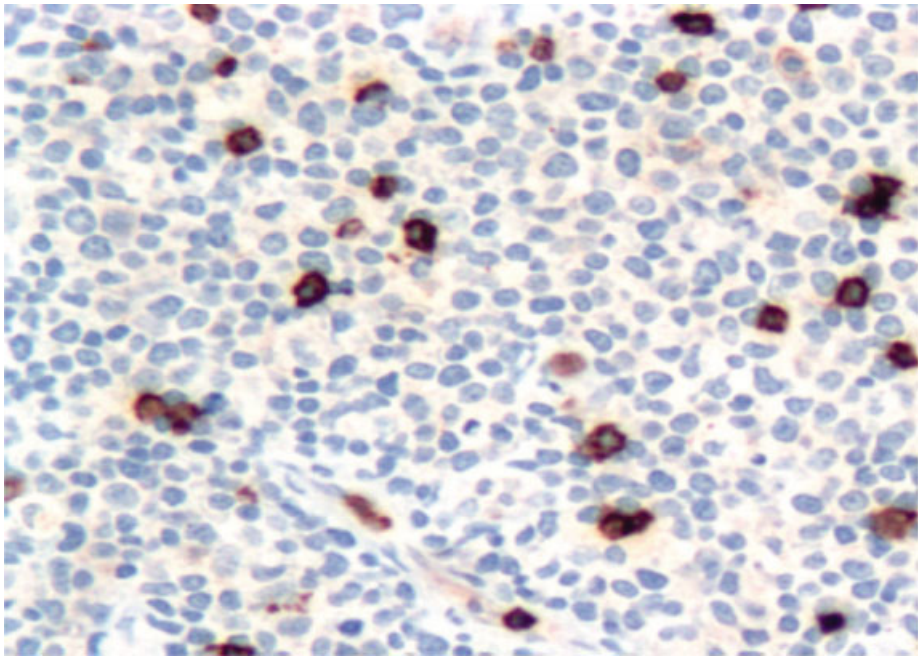

FIG. 1. Color image frame of CD8 + immunostained tumor infiltrating cell response and mantle cell lymphoma(Brown DAB and Blue Hematoxylin, 20×).

labeled COBs area converted to microns. Majority of COBs were circular. Circularity index averaged 95% for COBs in each image frame. A total of 2,027 image frames with 810,800 COBs were evaluated including prerun image frames to set the optimal microscope light intensity and configuration. TC, when using the 2–3 s per frame prototype, is extrapolated to a minute for a high throughput analysis, and using 500–600 cells per frame, the throughput is 15,000–18,000 cells per min.

Contrast—Validation of Experimental and Empiric Data

The blue channel and red channel intensity monochromatic images are shown in Figure 2. Note that by using the line tool and the resulting pixel density profile (inset), the brown stained COBs (arrow) show as higher contrast than the blue nuclei (asterisk) in the blue channel. In contrast, the red channel line profile shows both the brown and blue objects to be rather more uniformly visible and similar in pixel density. The profiles provided the numbers needed by the contrast equation. This visual appearance of difference in contrast was validated by using the contrast Eq. (5) shown above. Figures 2A and 2B show the images and plot profiles that provided data for the contrast calculation based on the images of blue and red channel.

As an example in the calculation of contrasts of COBs using blue and red channels only, Figure 2 data is shown below (0 is white and 255 is black):

1. the background average pixel density for blue and red channels (B, R) is 30;
2. I_{max} for brown objects are 191.85 and 185 for B and R channels, respectively;
3. I_{min} for blue objects are 50 and 110 for B and R channels, respectively;
4. the $I_{max} - I_{min}$ contrast difference between brown and blue COBs in blue and red channels were 141.85 and 75, respectively.

The results of contrast calculation for all the B, R, and G (blue, red, and green) channels between brown and blue objects including the background were 48%, 21%, and 36% respectively, where higher contrast obviously shows more difference than lower contrast percentage by visual display.

The data implies that:

1. brown objects yield the highest contrast versus blue objects in blue channel (48%);
2. blue objects yield a lower contrast versus brown objects in the red channel (21%);
3. brown objects yield an intermediate contrast versus blue objects in the green channel (36%).

These observations, based on these figures alone, suggest that to maximally differentiate between colored brown and blue COBs using contrast calculation, a 48% contrast was at the least necessary(Fig. 2A). A lower contrast (as low as 21%) implies inclusion of both the brown and blue objects as the target objects. This implication was validated by observing the gray scale appearance of these COBs in the red filter channel monochromatic intensity image (Fig. 2B). The green filter channel with a contrast calculated at 36% approximates the red filter result (picture not shown). The "no difference contrast" therefore lies theoretically between 21% and 36% and the "difference contrast" was close to or greater than 48%.

Concordance

The results of TC were compared with manual counts of expert observers and with the results of FC immuno-

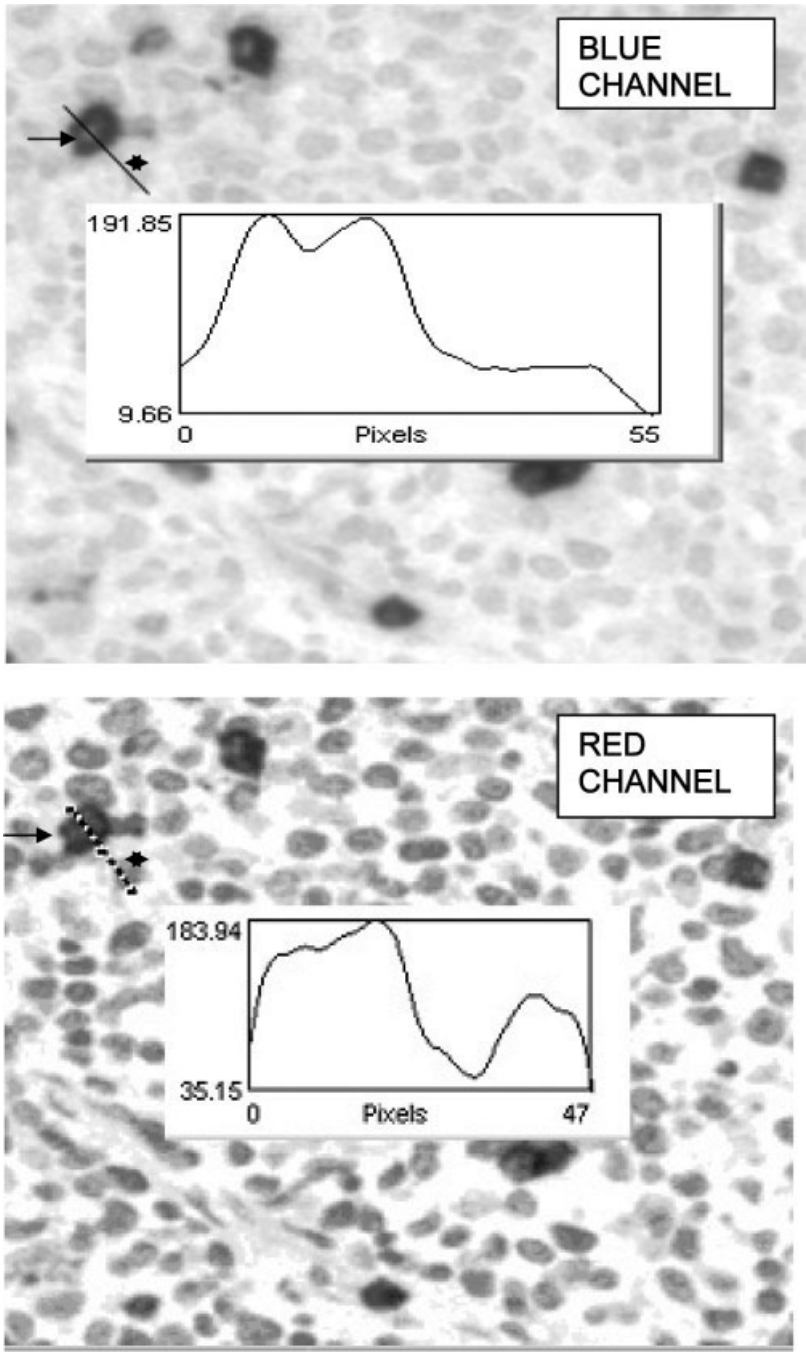

FIG. 2. Procedure for contrast calculation. Blue and red monochromatic channels displayed on the screen. A plot profile function and a line selector tool was used to draw a line from two COBs with intervening space for the background: one corresponding to the brown stained cell (arrow) and the other to the unstained nuclei (asterisk). The intensity numbers on Y were obtained and the I minimum of the COBs representing the brown stained cell were used for the calculation of the contrasts percent and I maximum of blue COBs were used. X was the pixel distance covered by line. The larger this contrast difference, the higher the percent contrast between the brown and blue objects.

phenotyping of the same specimen. Each of the dots in the two parameter analysis represents two observations where the value of TC is one axis and the corresponding axis is either a manual count or FC result. Some of the antibody like bcl-1 was not paired with a FC equivalent. The correlation coefficient and 95% confidence interval by linear regression analysis yielded a high concordance between manual human results (M), FC results, and TC results per antibody: (correlation coefficient $r = 0.93$ and linearity $r^2 = 0.8829$ manual vs. TC); (correlation coefficient $r = 0.96$ and linearity $r^2 = 0.9308$ FC vs. TC). The graphs of the regression analysis are shown in Figure 3. When compared with M and FC results, the concordance is high. The total cells analyzed by virtual FC is comparable to the total cells analyzed by flow cytometry. The average of 7.5 thousands cells analyzed per antibody indicates that the TC result is a high throughput methodology as well as that of flow cytometry.

Virtual Flow and FC Result

The brown and blue stained nuclei (Fig. 4A) are separately analyzed. Positive brown COBs are segmented and

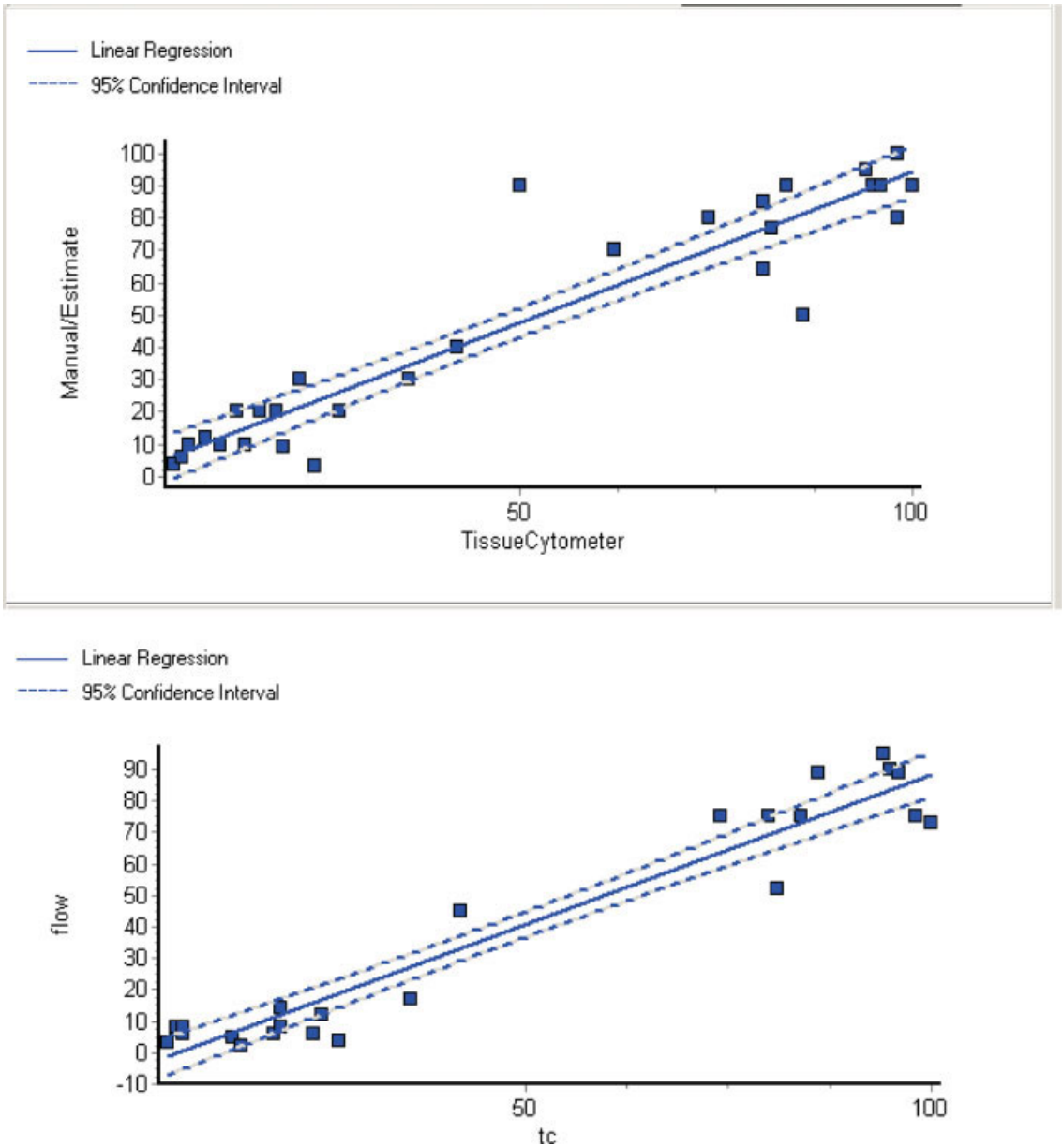

FIG. 3. The correlation coefficient and 95 % confidence interval by linear regression analysis yielded a high concordance between M ($r = 0.93$), FC results ($r = 0.9648$), and TC results, $P < 0.002$. [Color figure can be viewed in the online issue, which is available at www.interscience.wiley.com.]

used as the numerator (Fig. 4B). Negative COBs are added to positive COBs to give the total COBs. By cellular exclusive OR binary logic applied to color objects masks in Figure 4A, the brown and the blue nuclei are separated and the results are displayed in Figures 4C and 4D. The latter "events" are used as the denominator comprising the segmented brown stained CD8+ lymphocytes along with the unstained blue nuclei of non-CD8 tumor lymphocytes. The corresponding dot plot of the TC in Figure 4F shows the relative cell nuclear size (*Y*-axis) against the immunostaining density (*X*-axis) where the COBs size in microns and the relative stain density are linearly arrayed from 0 to 255. The blue stained negative COBs are close to zero and brown stained positive COBs are toward 255. The corresponding output in a table format shows staining density, total COBs population, positive COBs, percentage positive COBs in Figure 4G. The corresponding FC result is shown in Figure 4E displaying the FC dual parameter dotplot of forward side scatter versus CD8 intensity. The *Y*-axis indicates the size (forward side scatter) and the *X*-axis shows the CD8 fluorescence intensity (linear scale).

Second mode results. The 5% percentile thresholding when applied to only the blue COBs resulted in catching even the lowest stained blue nuclei, as shown in Figure 4C. The above procedures applying the combination of second percentile mode with the automated thresholding using χ

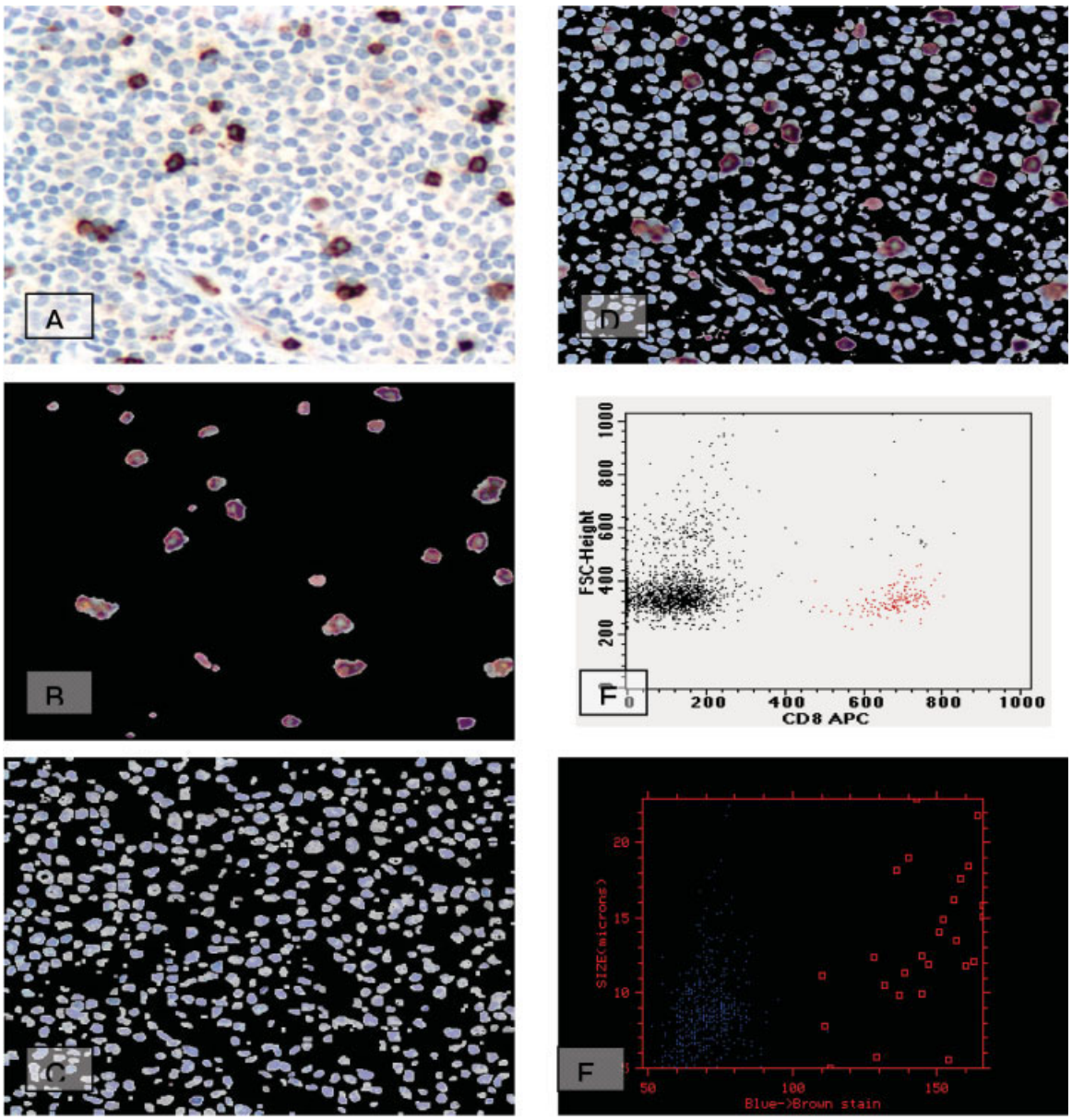

G

#	Leucocyte_den	Lymphocyte_num	Lymph_stain_num	Lymph_stain_ratio(%)
1	4	511	26	5.088063
Min	4.00	511	26	5.088063
Max	4.00	511	26	5.088063
Median	4.00	511	26	5.088063
Total		511	26	
Average	2.56	511.000000	26.000000	5.088063

The results have been saved in the user1:case1:lymphres.dat

FIG. 4. (**A**) Color image frame of CD8 + immunostained tumor infiltrating cell response and mantle cell lymphoma (brown DAB and blue hematoxylin, 20x). (**B**) Positive brown COBs segmented below (the numerator). (**C**) Negative COBs below were added to positive COBs to give the total COBs (the denominator). (**D**) Segmented brown stained CD8+ lymphocytes along with the unstained blue nuclei of non-CD8 tumor MC lymphocytes. (**E**) Flow cytometry: size (FSC) vs. CD8 fluorescence intensity (linear). (**F**) TC: size vs. staining density (linear) Cell Size in microns in Y and the Staining Density in X (0 to 255, where blue stain was close to zero and brown stain was toward 255). (**G**) Table showing staining density, total cell population, positive COBs, percentage positive COBs.

permitted maximal detection of all brown and blue COBs from the lowest to the highest intensity.

Third mode results. The third mode resulting from auto-thresholding applied to the histogram distribution of the selected image frame increased the sensitivity to parallel that seen with manual observation. One subroutine employed the isodata auto-thresholding mode to maximally catch the most intense-brown staining COBs and ignore the fuzzy brownish punctate background smudge around some of the brown stained COBs (Fig. 4A).

Another subroutine used entropy parameter passed from previous procedures and resulted in automated selection of brown stained objects invariant to transmitted light and staining intensity (data not shown). We have discovered that percent positive COBs varied in linear way based on the results of the equation for χ (data not shown). The value of χ, when applied to the thresholding of positive immunostained objects, linearly varies with the percent positive COBs.

The range of the χ parameter was adequate to decrease or increase the sensitivity for the brown staining COBs. The value of parameter for the entropy χ and the resulting thresholded objects account for both the variations of staining from densely dark brown to light brown pixels. Using the lower value for χ, i.e., 0.01, the fuzzy brownish stain in the intercellular areas was not included as an object (Fig. 4A). The dark brown COBs were the only ones included. The resulting objects were similar to COBs identified by the automated result of isodata thresholding mode.

With some of the antibodies, the true immunoreactivity shows a range of strong as well as a weak pattern (Fig. 5). Using the higher value for χ, i.e., 0.45, more of the weaker stained COBs were thresholded, including the COBs with weaker brown stain in addition to the darkly positive COBs. The maximum value for χ (close to 0.5) extended the range of object inclusion beyond the isodata mode thresholded objects. In Figure 5D, for example, the CD5 antibody had immunostained many lymphocytes in a weak cytoplasmic pattern as shown, with a distinct strong staining in only a few COBs. The results of thresholding with entropy value χ of 0.45 included also the weak stained COBs but entropy χ of 0.01 included only the darkly positive CD5 lymphocytes and ignored the weakly reactive COBs. The change in χ was translated as inclusion of more positive COBs including those with lower brown staining. The percentage increase of positivity was linear using χ from 0.01 to 0.49 and from few percent to close to 100% positive objects (data not shown).

Precision and Coefficient of Variation

The precision and accuracy using the above techniques were also determined by within run of the same tissue of the same antibody giving the coefficient of variation per antibody. A table of results from 10 to 24 image frames were obtained per slide per antibody. The coefficient of variation of TC ranged from 0.02 to 1.63 and averaged 1.40 and the COV between human operators was above 20% (data not shown). Sensitivity was determined by running the analysis per image frame and determining the rate of rare positively stained COBs detectability. Using 20× objective field of view, a 0.003–0.002 rare event sensitivity per frame was translated to 1/300–1/500 COBs. A 20-frame analysis yielded a theoretic 1/10,000 sensitivity. A single cell was recognized, segmented, counted, and statistically tabulated an average of 3/100 of a second. A negative control with all cells unstained yielded all negative cells. A full frame takes 12–15 s from acquisition to report using an old generation 100 MHz PowerPC CPU chip and from 2–3 s using a Pentium running 1.6 GHz CPU.

Correlated Immunostain and Dot Plots

In Figure 5, the correlated dot plot displays of size and staining density of several antibodies are shown. The CD3, Bcl-1, Ki-67, and CD5 IHC image frames and the corresponding plots on the right panels are shown. Note that this version of *i*HCFlow™ TC algorithm detects both nuclear and cytoplasmic/membranous staining pattern without modification to the program and displays an intuitive visual representation of the IHC image frames along with the percent positive result.

DISCUSSION

The *i*HCFlow™ TC fulfills the major Cytomics criteria (11) of (1) relating multiple parameters to each other, (2) within large population of cells, (3) on a single-cell basis, (4) on a quantitative and observer-independent manner. But unlike the other cytomics systems which use immunofluorescent tissue stains (11–13), the system differs in using routine IHC on tissue generating flow cytometry-like results.

This novel technology of "virtual flow cytometry" or automated cellular IHC may benefit pathologists, researchers, and scientists who use data derived from automated TC. By transforming IHC to a flow cytometry-like analysis and reporting, we present a singular methodology that has not been reported before in IHC image analysis literature. The *i*HCFlow™ Cytometry technique is robust, accurate, and fast. Because of its defined application in fixed immunostained tissue section only, we believe it will complement and be surrogate to FC results when fresh tissue is not otherwise available. The result is highly visual and akin to FC and provides both size and stain density population distribution at a glance. Like FC, which is a standard of clinical hematology practice, TC may supplant the often subjective immunostaining reporting in pathology and may also complement other fluorescence and laser-based technology like laser scanning cytometry (LSC) (1,12,14,15).

LSC is able to convert immunofluorescent cytologic preparation to give a FC histogram report. However, LSC has difficultly in analysis of tissue immunofluorescence because of overlapping cells and hence may be difficult to implement as single cell analysis in tissue sections. LSC nevertheless, has been applied to fresh tissue sections to quantitate in low power view, the tissue distribution of the lymphoid population with good results using multicolor dyes (1). A modification using confocal microscopy could obtain size and shape information in low power view (11–13), but likewise loses the common hematoxylin stained microscopic nuclear details familiar to most pathologists and research scientist. The latter information is retained in *i*HCFlow™.

A significant number of cases have tissue already fixed and embedded in paraffin and are not amenable to FC analysis, which requires fresh cell suspension of tissue.

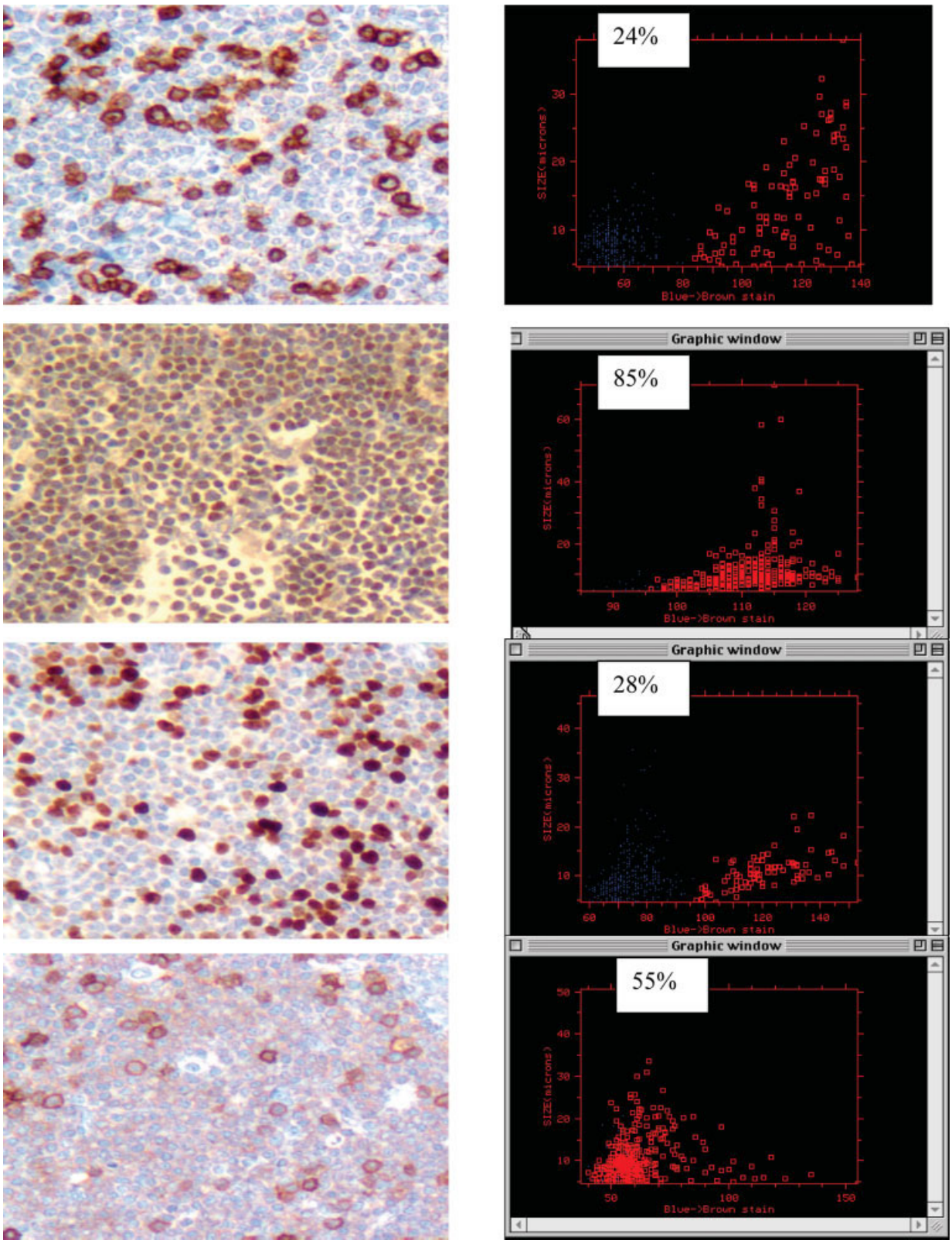

FIG. 5. Correlated immunostained images and corresponding dot plot TC results (cell size in microns versus staining density) for CD3, Bcl-1, Ki-67, and CD5, respectively.

Routinely in pathology practice, a panel of 5–15 IHC antibodies are applied to the slide-based tissue sections to create a result with a differential matrix to arrive at a correct diagnosis based on interpretation of tumor associated markers. The use of IHC often shift the diagnostic probability, especially in hematopathology, where an enhanced diagnostic accuracy is seen if the immunologic results are included. The enhanced accuracy is across the board where reported increased accuracy is noted from 5 to 35% of the cases (16). Most of diagnostic pathology, whether a small office or a large reference laboratory, use IHC as part of standard of practice. The few centers that have image analysis tools use those tools to quantitate antigen expression for hormone receptors for breast carcinoma prognosis (17) or for defined proliferative antigens (18,19) but not generally for counting positive COBs and getting the percentage.

FC uses viable and live cell suspension as well as immunofluorescence and laser light scattering methods, to obtain data and display results in a series of two dimensional histograms. We presented previously arguments that automation in FC could be used in diagnosis of hematologic malignancies (20–22). We extend this argument in the current presented data in automation of IHC results to virtual FC data which could also be useful in lymphoma diagnosis and monitoring.

Conversion of IHC to Flow Cytometry-Like Results

In this era of mature automated IHC instruments, we agree with a consensus report that the major problem in IHC standardization is not the staining quality but the interpretation (23). To contribute with IHC standardization and more objective interpretation of IHC, we identified several problems to overcome in order to obtain an accurate counting of immunostained cells in tissue: (1) thick sections with overlapping cells, (2) manual nonstandard immunostaining of tissues, (3) appropriate sampling resolution to give size and staining information per cell object, (4) lack of simple preprocessing technique to take advantage of the properties of image acquisition hardware, (5) lack of image specific thresholding algorithm to detect both the positive immunostained cells and nonimmunostained relevant cells of the same class, (6) lack of information on standardizing threshold cut off to compensate for variability in staining, and (7) lack of knowledge of which parameters or properties of IHC derived image are useful to automate thresholding.

We addressed the problems noted above individually and report on several novel approaches and techniques enabling performance of Tissue Cytometer:

1. Quality Histology: One of the problems in performing accurate manual or computerized image analysis count of nuclei in tissue section is ensuring reproducible high quality thin sections to minimize nuclei overlap (24). To accomplish TC with minimal overlap of nuclei and maximal nonreactive nuclei detection, we introduced two modifications in histology. We sectioned the lymph node tissue with microtome set at 2 μm and darkened the blue counterstain by extending the automated staining duration for 10 min. We believe these modifications are easily performed by current histotechnologists in many laboratories. These modifications have the additional effect of enhancing the overall quality of the microscopy sections.

2. We use an automated immunostaining and counterstaining platform for consistent, reliable, standardized processing along with the software protocol orchestrated by an industry standard system.

3. We obtained the sample of image at 20× magnification which provided optimal and adequate size resolution with more than enough pixels/micron for 10–12 μm average diameter fully satisfying the Nyquist sampling requirement (25) for adequacy of digital sampling.

4. Preprocessing suited to double thresholding: We report on a novel preprocessing step to automatically accentuate the contrast of positively stained COBs from nonstained COBs using the red and blue channel monochromatic images. These two channels are suitable for brown and blue colored objects and even reddish brown DAB or AEC combination (data not shown). We used differential enhancement of gray-scale using the built in RGB CCD and used the images with the highest contrast between objects and background. We preprocessed the images by CCD color channel dependent optical density contrast enhancement. Use of the Red and Blue channels increased the contrast and highlighted the brown pixels. The resultant proportion obtained was used in automating the thresholding of the various images to separate the brown objects (positive COBs) from the blue nuclei (negative COBs). The above technique and concept could be extended to any colored dye by employing tunable liquid crystal filters to adapt to any color or stain (26).

5. Normalizing staining by percentile thresholding. The application of the procedure of percentile thresholding has two appealing results. One, for cutting off dark and bright pixels from the intensity channel, the percentile thresholding stretched the histogram for enhanced contrast of COBs. Two, for hue channel cell objects, the hue singularity problem was reduced since the darkest and lightest color pixels were removed. The above procedure also converted the modulus property of hue to a linear array from 0 to 255 precluding complex calculations. The standard hue model is akin to a circular wheel where color property is measured in modular arithmetic. The measure becomes a practical issue since the color may be measured like the numbers in a clock with color values defined circularly in a repetitious manner.

6. We discovered the parameters obtained from the image itself to automate the thresholding function using the entropy mode. We found a good correlation between the ratio of positive COBs with negative COBs and the value of the parameter χ of entropy thresholding mode. We have not seen any report with a comparable parametrized study relating the positive cell ratio to a thresholding parameter that predicts percent results. A manual gating strategy as commonly employed in FC is also part of the

*i*HCFlow™ technique in selecting visually the positive cell population. The ability to have, in addition, a parameter for automation of this gating strategy is a major advantage over current automated immunohistochemical image analysis. A related approach of entropic thresholding of Tsallis is reviewed (27) but the latter results appear to pertain to the total grayscale image planes or image frames instead of the local region of interest (positive objects) as selected by χ parameter in this study.

How We Differ from Previous Studies

Previous studies have reported on using spectral capable instrumentation and wavelength filters (28); confocal immunofluorescent microscopy (12) to obtain separation of positive stain from nonstained pixels. Also a few hybrid microscope-FC were developed to obtain COBs information to mimic FC (29). Immunofluorescent techniques were applied on slide substrate (30) to obtain cell populations using laser scanning instrumentation. We believe our approach does not need the complex, fluorescent, and expensive instrumentation not readily available to a regular pathologist or oncologist. By using tools and techniques already available in many pathologists offices, we believe that the *i*HCFlow™ approach is sufficient to perform Virtual Flow Cytometry. Given an array of parameters that could be used to automate counting of positively stained COBs, we found that our approach of using density and color and size only as key information was able to do population reporting. The ability to convert the tissue immunostaining image to computerized data as a table of results and produce two-dimensional histograms: a virtual flow cytometer.

Approaches to Automate IHC Analysis

A number of reports addressed the issue of automated counting of immunostained cells in tissue using either a pixel area or cell-based analysis. Pixel area counts the pixels that are positive against the pixels that are negative and provides a ratio. Cell-based analysis groups the pixels according to defined characteristics and identifies the object corresponding to those pixels, labels them, and considers objects as events to be counted. In this way, objects of the same class are included to give a percent positive of the population. Most of the previous studies on counting immunohistochemical positive COBs are pixel-based (24,31–34). Population-based image analysis is more accurate, intuitive, and similar to the FC paradigm. Population-based analysis is more difficult and challenging than pixel-based techniques and only a few studies are seen (19,24,35,36). We have implemented a population-based image analysis with good results. Most of the previous approaches used pixel data to obtain the percent positive COBs or quantity of antigen present.

We noted a cell-based study similar to our approach in first obtaining the positive cells followed by the negative cells and getting a positive index or percent. Arambula used cell-based approach to determine index of positive cells with total cells using edge, color information with high predictive power but differs from our study in its technique and the lack of conversion to a flow cytometry-like results (36).

A few studies given below used different approaches yet no study performed automatic detection of positive cells using imaging CCD enhancement and automated gating by entropy fraction, as well as using size and intensity information as we did. Ranefall et al. used pixel ratio of positive objects to classify cells (37). Loukas et al. used cell-based analysis for Ki-67 and Cyclin A in squamous carcinoma of neck region (19). Karlsson et al. counted immunostained lymphocytes using CD4, CD8, CD20, CD23, and CD25 in frozen tissue sections by image analysis (38). Hilbe et al. (39) compared automated cellular imaging with manual microscopy using p53, ki-67, and p120 in frozen section by pixel area. Johansson et al. (33) looked at leukocytes infiltrating rat brain tumor using immunostaining and computerized image analysis. Using spectral ratio of stained and unstained COBs pixels Ornerg (24,28), quantitation of object areas is obtained. Elie et al. (40) counted immunostained nuclei using cyclin A by detecting positive pixels and ratio of stained area and total pixel of epithelia of human ovarian adenocarcinomas. These studies are different from the present report because none of these studies translated their results to a virtual FC paradigm with two-dimensional scatter histogram showing correlating cell size and cell staining density information.

Approaches to Segmentation

The generic method in extracting information from an image is by segmentation—divide the image into component objects or regions. Two major approaches in segmentation use the property of color and gray level values of objects: discontinuity and similarity. Objects with well-defined discontinuities usually benefit from edge-based detection, while those with poorly defined discontinuities may benefit from similarity approach such as thresholding. Because of the complex, discontinuous, multicolor, large scale images in immunohistochemically stained biologic cells (19) (33), a number of studies used the thresholding and pixel mask thresholding technique and because of similar accuracy issues have not implemented cell-based reporting. Accurate segmentation remains one of the problems in pixel mask image ratio with up to 15% error on both falsely positive and falsely negative results (USPTO patent No. 6,553,135).

We also wanted to correlate the TC results with the result of FC and manual counting to determine if the technique could be a surrogate to those currently in use. The correlation between each case run in flow cytometry, manually counted by experts, and by TC is high and suggest that this may be a surrogate and therefore a valid approach to diagnosis. This provides an automated method of image analysis portraying cell population statistics, in a greatly improved manner over manual scoring techniques. By combining the scientific advantages of automation and our methodology, as well as the greatly increased speed, we have created a high throughput technology by which pop-

ulations can be evaluated. The *i*HCFlow™ technique is a major improvement over methods currently available.

ACKNOWLEDGMENTS

Mantle Cell Lymphoma Task Force (J. Tao, E. Sotomayor, S. Dessureault, H. Molina, J. Balasi, G. Shaheen HISTOLOGY FLOW CYTOMETRY, MOFFITT).

LITERATURE CITED

1. Gerster AO, Trumpfheller C, Racz P, Osmancik P, Tenner-Racz K, Tarnok A. Quantitative histology by multicolor slide-based cytometry. Cytometry A 2004;61:210–219.
2. Miller MJ, Safrina O, Parker I, Cahalan MD. Imaging the single cell dynamics of CD4+ T cell activation by dendritic cells in lymph nodes. J Exp Med 2004;200:847–856.
3. Kriete A. Bridging biological scales by state-space analysis and modeling using molecular, tissue cytometric and physiological data. Cytometry A 2006;69:113–116.
4. Kriete A, Boyce K. Automated tissue analysis—A bioinformatics perspective. Methods Inf Med 2005;44:32–37.
5. Kriete A, Anderson MK, Love B, Freund J, Caffrey JJ, Young MB, Sendera TJ, Magnuson SR, Braughler JM. Combined histomorphometric and gene-expression profiling applied to toxicology. Genome Biol 2003;4:R32.
6. Mouroutis T, Roberts SJ, Bharath AA. Robust cell nuclei segmentation using statistical modeling. Bioimaging 1998;6:79–91.
7. Zhang Y, Goldszal A, Butman J, Choyke P. Improving image contrast using principal component analysis for subsequent image segmentation. J Comput Assist Tomogr 2001;25:817–822.
8. Rea M. Solving the problem of VDT reflections. Prog Arch 1991;72:35–40.
9. Johannsen G, Bille J. A threshold selection method using information measures. Proc 6th Int Conf Pattern Recognit 1992;1092:140–142.
10. Vincent L, Soille P. Watersheds in Digital spaces: An efficient algorithm based on immersion simulations. IEEE Trans Pattern Anal Mach Intell 1991;13:583–598.
11. Ecker RC, Steiner GE. Microscopy-based multicolor tissue cytometry at the single-cell level. Cytometry A 2004;59:182–190.
12. Ecker RC, Tarnok A. Cytomics goes 3D: Toward tissomics. Cytometry A 2005;65:1–3.
13. Ecker RC, de MR, Steiner GE, Schmid JA. Application of spectral imaging microscopy in cytomics and fluorescence resonance energy transfer (FRET) analysis. Cytometry A 2004;59:172–181.
14. Sack U, Bocsi J, Tarnok A. Slide-based cytometry and predictive medicine: The 8th Leipziger workshop and the 1st international workshop on slide-based cytometry. Cytometry A 2004;60:189–205.
15. Valet G, Tarnok A. Potential and challenges of a human cytome project. J Biol Regul Homeost Agents 2004;18:87–91.
16. Anonymous. The non-Hodgkin's lymphoma classification project: A clinical evaluation of the international lymphoma study group classification of non-Hodgkin's lymphoma. Blood 1997;89:3909–3918.
17. Czerniak B, Herz F, Wersto RP, Alster P, Puszkin E, Schwarz E, Koss LG. Quantitation of oncogene products by computer-assisted image analysis and flow cytometry. J Histochem Cytochem 1990;38:463–466.
18. Caulet S, Lesty C, Raphael M, Schoevaert D, Brousset P, Binet JL, Diebold J, Delsol G. Comparative quantitative study of Ki-67 antibody staining in 78 B and T cell malignant lymphoma (ML) using two image analyser systems. Pathol Res Pract 1992;188:490–496.
19. Loukas CG, Wilson GD, Vojnovic B, Linney A. An image analysis-based approach for automated counting of cancer cell nuclei in tissue sections. Cytometry A 2003;55:30–42.
20. Cualing H, Kothari R, Balachander T. Immunophenotypic diagnosis of acute leukemia by using decision tree induction. Lab Invest 1999; 79:205–212.
21. Cualing HD. Automated analysis in flow cytometry. Cytometry 2000; 42:110–113.
22. Kothari R, Cualing H, Balachander T. Neural network analysis of flow cytometry immunophenotype data. IEEE Trans Biomed Eng 1996;43: 803–810.
23. Rudiger T, Hofler H, Kreipe HH, Nizze H, Pfeifer U, Stein H, Dallenbach FE, Fischer HP, Mengel M, Von WR, Muller-Hermelink HK. Quality assurance in immunohistochemistry: Results of an interlaboratory trial involving 172 pathologists. Am J Surg Pathol 2002;26:873–882.
24. Ornberg RL. Proliferation and apoptosis measurements by color image analysis based on differential absorption. J Histochem Cytochem 2001; 49:1059,1060.
25. Young IT. Sampling density and quantitative microscopy. Anal Quant Cytol Histol 1988;10:269–275.
26. Morris HR, Hoyt CC, Miller P, Treado PJ. Liquid Crystal tunable filter Raman chemical imaging. Appl Spectrosc 1996;50:805–811.
27. Portes de Albuquerque M, Esquef IA, Gesualdi Mello AR. Image thresholding using Tsallis entropy. Pattern Recognit Lett 2004;25:1059–1065.
28. Ornberg RL, Woerner BM, Edwards DA. Analysis of stained objects in histological sections by spectral imaging and differential absorption. J Histochem Cytochem 1999;47:1307–1314.
29. Wietzorrek J, Plesnila N, Baethmann A, Kachel V. A new multiparameter flow cytometer: Optical and electrical cell analysis in combination with video microscopy in flow. Cytometry 1999;35:291–301.
30. Galbraith W, Wagner MC, Chao J, Abaza M, Ernst LA, Nederlof MA, Hartsock RJ, Taylor DL, Waggoner AS. Imaging cytometry by multiparameter fluorescence. Cytometry 1991;12:579–596.
31. Brey EM, Lalani Z, Johnston C, Wong M, McIntire LV, Duke PJ, Patrick CW Jr. Automated selection of DAB-labeled tissue for immunohistochemical quantification. J Histochem Cytochem 2003;51:575–584.
32. Brey EM, King TW, Johnston C, McIntire LV, Reece GP, Patrick CW Jr. A technique for quantitative three-dimensional analysis of microvascular structure. Microvasc Res 2002;63:279–294.
33. Johansson AC, Visse E, Widegren B, Sjogren HO, Siesjo P. Computerized image analysis as a tool to quantify infiltrating leukocytes: A comparison between high- and low-magnification images. J Histochem Cytochem 2001;49:1073–1079.
34. Sont JK, De Boer WI, van Schadewijk WA, Grunberg K, van Krieken JH, Hiemstra PS, Sterk PJ. Fully automated assessment of inflammatory cell counts and cytokine expression in bronchial tissue. Am J Respir Crit Care Med 2003;167:1496–1503.
35. Dahle J, Kakar M, Steen HB, Kaalhus O. Automated counting of mammalian cell colonies by means of a flat bed scanner and image processing. Cytometry A 2004;60:182–188.
36. Arambula CF, Marquez Flores JA, Padilla Castaneda MA, Solano S, Tato P. Automatic analysis of immunocytochemically stained tissue samples. Med Biol Eng Comput 2005;43:672–677.
37. Ranefall P, Egevad L, Nordin B, Bengtsson E. A new method for segmentation of colour images applied to immunohistochemically stained cell nuclei. Anal Cell Pathol 1997;15:145–156.
38. Karlsson MG, Davidsson A, Hellquist HB. Quantitative computerized image analysis of immunostained lymphocytes. A methodological approach. Pathol Res Pract 1994;190:799–807.
39. Hilbe W, Gachter A, Duba HC, Dirnhofer S, Eisterer W, Schmid T, Mildner A, Bodner J, Woll E. Comparison of automated cellular imaging system and manual microscopy for immunohistochemically stained cryostat sections of lung cancer specimens applying p53, ki-67 and p120. Oncol Rep 2003;10:15–20.
40. Elie N, Plancoulaine B, Signolle JP, Herlin P. A simple way of quantifying immunostained cell nuclei on the whole histologic section. Cytometry A 2003;56:37–45.